# Inferred Vehicular Emissions at a Near-Road Site: Impacts of COVID-19 Restrictions, Traffic Patterns, and Ambient Air Temperature

Dolly L. Hall-Quinlan[1], Hao He[1,2], Xinrong Ren[1,3], Timothy P. Canty[1,4], Ross J. Salawitch[1,2,5], Phillip Stratton[1], Russell R. Dickerson[1,2,5]

[1] Department of Atmospheric and Oceanic Science, University of Maryland, College Park, Maryland, USA

[2] Earth System Science Interdisciplinary Center, University of Maryland, College Park, Maryland, USA

[3] Air Resources Laboratory, National Oceanic and Atmospheric Administration, College Park, Maryland, USA

[4] Marine Estuarine Environmental Sciences, University of Maryland, College Park, Maryland, USA

[5] Department of Chemistry and Biochemistry, University of Maryland, College Park, Maryland, USA

*Correspondence to*: Dolly Hall-Quinlan (dahall01@umd.edu)

Keywords: On-road Emissions; Air Quality; COVID-19; Ambient Temperature; Emission Model; Black Carbon; $NO_x$; CO; $CO_2$

**Abstract**

Vehicles are a major source of anthropogenic emissions of carbon monoxide (CO), nitrogen oxides ($NO_x$), and black carbon (BC). CO and $NO_x$ are known to be harmful to human health and contribute to ozone formation, while BC absorbs solar radiation that contributes to global warming and also has negative impacts on human health and visibility. Travel restrictions implemented during the COVID-19 pandemic provide researchers the opportunity to study the impact of large, on-road traffic reductions on local air quality. Traffic counts collected along Interstate-95, a major eight-lane highway in Maryland (US), reveal a 60% decrease in passenger car totals and an 8.6% (combination-unit) and 21% (single-unit) decrease in truck traffic counts in April 2020 relative to prior Aprils. The decrease in total on-road vehicles led to the near-elimination in stop-and-go traffic and a 14% increase in the mean vehicle speed during April 2020. Ambient near-road (NR) BC, CO, $NO_x$, and carbon dioxide ($CO_2$) measurements were used to determine vehicular emission ratios ($\Delta BC/\Delta CO$, $\Delta BC/\Delta CO_2$, $\Delta NO_x/\Delta CO$, $\Delta NO_x/\Delta CO_2$, and $\Delta CO/\Delta CO_2$), with each ratio defined as the slope value of a linear regression performed on the concentrations of two pollutants within an hour. A decrease of up to a factor of two in $\Delta BC/\Delta CO$, $\Delta BC/\Delta CO_2$, $\Delta NO_x/\Delta CO_2$, and in the fraction of on-road diesel vehicles from weekdays to weekends shows diesel vehicles to be the dominant source of BC and $NO_x$ emissions at this NR site. We estimate up to a 70% reduction in BC emissions in April 2020 compared to earlier years, and attribute much of this to lower diesel BC emissions resulting from improvements in traffic flow and fewer instances of acceleration and braking. Future efforts to reduce vehicular BC emissions should focus on improving traffic flow or turbocharger lag within diesel engines. Inferred BC emissions from the NR site also depend on ambient temperature, with an increase of 54% in $\Delta BC/\Delta CO$ from −5 to 20 °C during the cold season, similar to

previous studies that reported increasing BC emissions with rising temperature. The default setting of MOVES3, the current version of the mobile emission model used by the US EPA, does not adjust hot-running BC emissions for ambient temperature. Future work will focus on improving the accuracy of mobile emissions in air quality modeling by incorporating the effects of temperature and traffic flow in the system used to generate mobile emissions input for commonly used air quality models.

## 1. Introduction

Vehicles emit substantial amounts of carbon monoxide (CO), nitrogen oxides ($NO + NO_2 = NO_x$), black carbon (BC), and carbon dioxide ($CO_2$). Both CO and $NO_2$ are criteria pollutants regulated by the United States Environmental Protection Agency (US EPA) due to their hazards to human health and role as precursors to the formation of ozone, $O_3$ (Crutzen, 1973; Pusede & Cohen, 2012; Sather & Cavender, 2016). Fine particulate matter ($PM_{2.5}$), defined as "particulate matter with a nominal mean aerodynamic diameter less than or equal to 2.5 μm" (US EPA, 2016), includes BC and all other particulate matter in this size range, and is regulated by the US EPA due to the adverse health and visibility impacts (US EPA, 2021b). Ozone, BC, and $CO_2$ absorb radiation and can have adverse radiative forcing (US EPA, 2021a).

According to the 2017 National Emissions Inventory (NEI), the mobile sector is the dominant emitter of CO and $NO_x$ both nationally and within Maryland (US), the focus of this study. At the national scale, vehicles contribute to 44% of total CO (including wildfires) and 52% of total $NO_x$ emissions, and in Maryland vehicles generate 83% of total CO and 70% of total $NO_x$ emissions. The mobile sector is also the largest contributor to BC emissions, representing 42% of total emissions nationally and 58% in Maryland. Within the on-road mobile

68 sector in Maryland, diesel engines are estimated to emit 75% of BC, 41% of $NO_x$, but only 3.8%
69 of CO, with similar percentages on the national scale (US EPA, 2022).

70 Lockdown mandates and other restrictions imposed in response to the COVID-19 public
71 health emergency in early 2020 resulted in a sharp decline in the number of on-road vehicles, a
72 decrease in traffic congestion, and lower vehicular emissions (e.g., Du et al., 2021; Harkins et al.,
73 2021; Hudda et al., 2020; Laughner et al., 2021; Yang et al., 2021) and other sources (e.g., Ahn
74 et al., 2022; Gaubert et al., 2021; Krüger et al., 2022; Lopez-Coto et al., 2022; Yadav et al.,
75 2021; Zeng et al., 2022).

76 Diesel-fueled trucks and gasoline-fueled cars emit air pollutants in varying amounts
77 (Grieshop et al., 2006; Hudda et al., 2020), primarily due to differences in engine technologies
78 used by each type of vehicle. Diesel engines inject the fuel directly into the engine cylinders
79 (known as direct injection) and tend to operate fuel-lean, while gasoline engines typically premix
80 the air and fuel upstream of the engine cylinders and operate at lower air-to-fuel ratios and lower
81 maximum temperature. The latter process results in higher emissions of CO and lower emissions
82 of BC and $NO_x$ for gasoline compared to diesel-fueled vehicles (Ban-Weiss et al., 2008; Park et
83 al., 2011).

84 To study emissions from gasoline and diesel vehicles in the near-road (NR) environment,
85 here we use emission ratios, such as $\Delta NO_x/\Delta CO_2$, to indicate the amount of $NO_x$ emitted ($\Delta NO_x$,
86 where $\Delta$ represents the change in concentration relative to the background) relative to the amount
87 of $CO_2$ emitted ($\Delta CO_2$). Emission ratios are useful to interpret the relative influence of gasoline
88 and diesel vehicles in an air sample because each source has its own unique range of emission
89 ratios. For example, exhaust emissions from diesel trucks contain approximately ten times
90 higher $\Delta NO_x/\Delta CO_2$ emission ratios because diesel vehicles produce more $NO_x$ than gasoline

vehicles and diesel engines typically run with greater fuel efficiency, resulting in lower $CO_2$ than from a gasoline engine of comparable size (O'Driscoll et al., 2018). $\Delta NO_x/\Delta CO$ emission ratios from diesel-fueled compression-ignited vehicles (CIVs) are typically close to 1 and for gasoline-fueled spark-ignited vehicles (SIV) the ratios are closer to 0.1 (Bureau of Transportation Statistics, 2018). Fuel-specific BC emission factors ($g_{BC}/kg_{fuel}$) from CIVs are up to 50 times higher than those from light-duty SIVs (Ban-Weiss et al., 2008; Dallmann et al., 2013), while CO emission factors are roughly half of those from SIVs (Dallmann et al., 2013).

Vehicle speed and acceleration affects vehicular emissions of BC, CO, and $NO_x$. Turbocharger lag, resulting from acceleration in diesel vehicles, produces a mixture of BC, metals, unburnt fuel and oil, and sulfates, a blend commonly referred to as soot (Rakopoulos & Giakoumis, 2009). Therefore, fewer instances of acceleration result in lower BC emissions (Giakoumis & Zachiotis, 2021). Prior work shows conflicting results of the effect of driving cycles on emissions. For example, PM emissions showed no clear trend with driving cycle in Dixit et al. (2017) and Durbin et al. (2008). Using dynamometer data, Dixit et al. (2017) showed that $NO_x$ emissions from heavy-duty (HD) diesel trucks were often more than twice as high for a stop-and-go driving cycle as for free-flow traffic. $NO_x$ emissions were also uniformly higher when exhaust aftertreatment systems (designed to remove $NO_x$) were below the optimal operating temperature; see also (Jiang et al., 2022; McCaffery et al., 2021). These studies were focused on urban driving cycles and are not strictly comparable to traffic on an interstate highway where a substantial fraction of the vehicles move at speeds exceeding 27 m $s^{-1}$ (for reference, 1 m $s^{-1}$ equals 2.2 miles $hr^{-1}$). Prior studies also indicate that some, but not all, HD vehicles show higher $NO_x$ emissions (per distance traveled) for the higher cruise speeds (> 24.5 m $s^{-1}$) than for 18 m $s^{-1}$ cruise (Durbin et al., 2008). Batterman et al. (2010) found emissions of

114 $NO_x$ and CO (per distance traveled) to vary by speed for the combined vehicle fleet, with
115 emissions increasing with speeds above 18 m $s^{-1}$.

116 Ambient temperature has been found to impact on-road vehicular emissions (Bishop et
117 al., 2022; Grange et al., 2019; Hall et al., 2020; Li & Lü, 2021; Saha et al., 2018; Weber et al.,
118 2019). Inferred mobile $NO_x$ emissions at a NR site in Maryland were lower at higher outdoor
119 temperatures while CO and $CO_2$ emissions remained relatively constant (Hall et al., 2020). A
120 similar temperature sensitivity was reported at a NR site in North Carolina (US), with higher
121 $NO_x$ emission factors in winter than in summer (Saha et al., 2018). Further studies examining
122 the European vehicle fleet found declining mobile $NO_x$ emissions with rising ambient
123 temperatures in light-duty diesel vehicles (Grange et al., 2019; Weber et al., 2019). Some
124 publications suggest that mobile BC emissions peak at the highest ambient temperatures in
125 diesel-fueled vehicles (Book et al., 2015; Chen et al., 2001; Kondo et al., 2006) and in
126 "measureable emitters" (Wang et al., 2018). Other studies found little seasonal difference in the
127 contribution of total $PM_{2.5}$ mass concentration from diesel vehicles (Kim & Hopke, 2012);
128 gasoline-powered vehicles may even emit higher BC emissions at colder temperatures, such as
129 during cold-starts (Schauer et al., 2008).

130 Impacts of ambient temperature on vehicular emissions need to be properly represented
131 in mobile emissions models and inventories. The NEI estimates mobile emissions using the
132 MOtor Vehicle Emissions Simulator (MOVES) developed by the US EPA (US EPA, 2015b) that
133 incorporates multiplicative factors to adjust mobile hot-running emissions of CO, $NO_x$, and BC
134 for ambient temperature. In both the previous version (MOVES2014b) and the latest version
135 (MOVES3), the adjustment factors for CO and $NO_x$ are set to unity and running emissions from
136 any gasoline- or diesel-powered vehicle are commonly not adjusted for temperature (US EPA,

2015a, 2020a). MOVES2014b includes an adjustment for hot-running BC emissions for gasoline vehicles of model year (MY) 2004 and earlier but does not modify running BC emissions from diesel-fueled vehicles (US EPA, 2015a). The temperature sensitivity in running BC emissions from MY 2004 and older gasoline vehicles was removed in MOVES3 (US EPA, 2020a); see also Hall et al. (2020). The absence of a temperature sensitivity in mobile BC emissions simulated by MOVES may also help to explain a previous study showing that the CMAQ model, which indirectly uses mobile emissions simulated by MOVES, underestimates ambient BC concentrations in the summer but not in the winter (Appel et al., 2008).

In this study we use ambient measurements of BC, CO, $NO_x$, and $CO_2$ collected at a fixed NR site located along Interstate-95 (I-95) in Maryland to infer mobile emissions using ratios of these measurements. Our goal is to quantify the impact of changes in on-road vehicle fleet composition and the near-elimination in traffic jams on highway emissions. We also present evidence for a temperature dependence in mobile BC emissions and compare the results to the temperature sensitivity of BC emissions from MOVES3.

## 2. Methodology

### 2.1 Interstate-95 Near-Road and Traffic Observations

Ambient pollutant concentrations and meteorological data were measured at a NR site located 12 m from the southbound leg of I-95, an eight-lane interstate highway in Howard County, Maryland (MD, Figure S1; 39° 8’ 35.38” N, 76° 50’ 45.53” W). Observations were collected between January 2017 and December 2018, then again from March 2020 through December 2020. The site is managed by the Maryland Department of the Environment (MDE) as part of the US EPA Air Quality System (AQS), and the monitoring site follows standard

measurement collection and quality control protocol outlined in the Code of Federal Regulations (CFR) 40 part 58 (available at http://www.ecfr.gov/cgi-bin/ECFR?page=browse). Hourly-mean data were calculated from 10-second mean $NO_x$ and CO mixing ratios, 1-minute mean BC concentrations ([BC]), and 2-second mean $CO_2$ abundances. The measurement technique, analyzer used, and relative accuracy of the CO, $NO_x$, $CO_2$, BC, and meteorological measurements are provided in Table 1 and discussed in more detail in Section S1 of the Supplemental Information (SI). To isolate highway emissions, only hours when winds were blowing from the adjacent highway (25° to 225° clockwise from North) were used in these analyses. Allowing wind from all directions had little impact on the results.

**Table 1.** Instrument details for the CO, $NO_x$, BC, $CO_2$, and meteorological variables measured at the I-95 NR site used in this study. The accuracy is provided as a relative value with the appropriate reference given.

| Pollutant Species | Method of Detection/Analyzer | Accuracy |
|---|---|---|
| CO | Infrared Energy Absorption<br>Teledyne API 300U | 2.3%<br>(See the SI) |
| $NO/NO_2/NO_x$ | Chemiluminescence<br>Teledyne API 200U | 4.7%<br>(See the SI) |
| BC | Filter-based, optical measurement technique<br>Magee Scientific TAPI M633 (AE33)<br>Aethalometer (880 nm) | ~ 5%<br>(Grimes & Dickerson, 2021) |
| $CO_2$<br>(2017 and 2018) | Laser Absorption Spectroscopy<br>Los Gatos Research Fast Greenhouse Gas Analyzer | 0.089%<br>(See the SI) |
| $CO_2$<br>(2020) | Laser Absorption Spectroscopy/Cavity Ring-down<br>Picarro Model G2301 | 0.025%<br>(See the SI) |
| T/P/RH/Winds | Vaisala WXT 520 | T: 0.3 °C<br>P: 0.5-1 hPa<br>RH: 3-5%<br>WS: 3-5%<br>WD: 3°<br>(Vaisala, 2012) |

Hourly traffic observations along I-95 were collected by an in-road traffic sensor, operated by the Maryland State Highway Administration. The sensor is located 8 km north of the ambient NR trailer and had a daily mean of 198,000 passing vehicles prior to March 2020. Vehicle information (count, type, and speed) was measured using a combination of two inductive loops and a class II piezo pressure sensor in each lane to count the number of and spacing between vehicle axles. This technique allows the site to count the hourly total number of vehicles, as well as vehicle type and speed from the number of and distance between axles (US Department of Transportation Federal Highway Administration, 2014). The sensors connect to an electronic equipment cabinet adjacent to the highway that contains two Diamond Traffic Products Phoenix II Classifiers with Integrated IRIS cellular modems to record the vehicle data.

## 2.2 Inferred Emission Ratios and Speed and Temperature Sensitivity Analysis

The proximity of the I-95 NR site to the highway provides an ideal setting to analyze mobile emissions. BC, CO, $NO_x$, and $CO_2$ share vehicles as a common source, resulting in similar patterns for ambient measurements of BC, CO, $NO_x$, and $CO_2$ in the NR environment (see, for example, Krecl et al. [2018] and Naser et al. [2009]). Covariations in pollutants are useful to study properties in vehicular emissions through inferred emission ratios, which are often applied to trace specific sources in plume analysis. Here we calculate the hourly $\Delta BC/\Delta CO$, $\Delta BC/\Delta CO_2$, $\Delta NO_x/\Delta CO$, $\Delta NO_x/\Delta CO_2$, and $\Delta CO/\Delta CO_2$ emission ratios from the slope parameter of linear geometric mean regression fits performed on five-minute mean mixing ratios of two pollutants sampled within that hour, similar to Anderson et al. (2014) and Hall et al. (2020). For example, the regression slope of five-minute mean [BC] and [CO] represents the hourly $\Delta BC/\Delta CO$. Only hours with more than 30 minutes of observations were used in the

198 analysis. Table S1 in the SI shows good agreement between fuel-based BC and $NO_x$ emission
199 factors calculated from the emission ratios in this study and emission factors reported in other
200 references.

201 To investigate the relative importance of CIVs and SIVs to the traffic flow and
202 temperature sensitivity in each time period, the analysis was performed for all days and hours, as
203 well as by weekday and time-of-day (overnight, morning rush hours, and afternoon rush hours).
204 We use Eastern Local Time (ET) for the analysis by hour of day, which is Eastern Standard Time
205 from early-November to mid-March and daylight savings for the remainder of the year.

206

207 **2.3 MOVES3 Temperature Sensitivity Simulations**

208 The latest version of the US EPA MOVES model, MOVES3, was used to simulate mobile
209 emissions for Howard County, MD. At the county-level scale, MOVES3 requires county-
210 specific input data including vehicle speed, road type, and age distributions; vehicle miles
211 traveled (VMT) by vehicle group, hour, day, and month; an average 24-hour profile of
212 temperature and relative humidity; vehicle population; inspection and maintenance; and fuel
213 information (see Table S2). All input, except for fuel information, was supplied by the MDE.
214 For input on fuel specifics, MOVES3 default data for Howard County, MD, was used as this
215 information had not yet been finalized by MDE at the time of paper submission.

216 MOVES3 emissions were generated in the form of emission rates, representing the mass
217 of pollutant per distance traveled. Emission rates generated by MOVES are a function of month,
218 temperature, relative humidity, vehicle type, fuel, speed, road type, model year, and
219 weekday/weekend. The choice of month impacts emission rates because the fuel information

used by MOVES3 differs between winter and summer. A major difference between summer and winter months in the model and in the real-world is the volatility of the fuel, with winter fuel used from September through April and summer fuel used from May through August (US EPA, 2021c).

In this study, MOVES3 simulations were performed using 2017 input data, the latest year with available data, and for the month of December, when winter gasoline and diesel fuels are used. Repeating the analysis for summer yields little difference in emission ratios (Figure S3). A detailed explanation of how weighted mean emission ratios were calculated using fleet composition data along I-95 is provided in Hall et al. (2020).

MOVES3 does not incorporate a temperature adjustment for hot-running BC emissions from either CIVs or SIVs. While neither MOVES3 nor the previous version, MOVES2014, adjusts hot-running BC emissions from CIVs, the default setting of MOVES2014 incorporates an adjustment for running BC emissions from pre-2004 model year SIVs for temperature, using a multiplicative adjustment factor (US EPA, 2015a, 2020a). To verify the documented absence of a temperature sensitivity in MOVES3 output, weighted mean emission ratios were calculated in 1 °C increments from −5 °C to 25 °C and the results presented in Section 3.2.

## 3. Results and Discussion

### 3.1 Impact of COVID-19 Traffic Restrictions on Vehicle Fleet, Traffic Flow, and Emissions

#### 3.1.1 Vehicle Fleet Characteristics Before and During the Pandemic

Travel restrictions for the COVID-19 pandemic began in mid-March 2020 in the Baltimore-Washington Region (BWR) and led to a peak decrease in on-road vehicle counts in

April 2020 (Figures 1 and S4). The mean daily total number of vehicles passing the site was 192,000 pre-COVID (April 2017 and 2018) and decreased to 96,300 in April 2020. Light-duty passenger vehicle counts were 60% lower in April 2020 relative to pre-COVID counts, while the number of buses was down by 85%, single-unit trucks by 21%, and trailer (combination-unit) trucks by 8.6% (Figure 1).

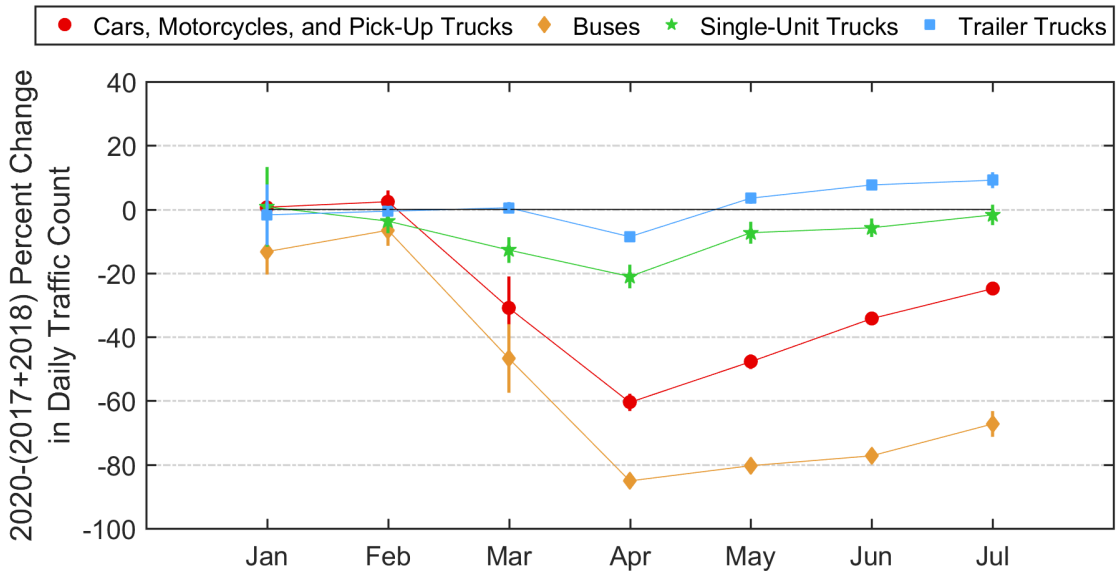


**Figure 1.** Relative difference (%) in monthly 2020 traffic counts compared to 2017 and 2018 for the months of January through July at the I-95 NR site. Error bars represent the 95% confidence intervals (2σ) of the mean daily traffic count differences in each month.

Of the vehicles passing the traffic sensor, the typical pre-COVID fleet composition was 88% cars, motorcycles, and light-duty pick-up trucks; 1.3% buses; 3.0% single-unit trucks; and 7.7% tractor-trailer trucks. The highest fraction of CIVs (single-unit and tractor-trailer trucks) typically occurred overnight from 23:00 to 4:59 ET, with a mean value (± 1σ) of 0.22 ± 0.072 (Table 2 and Figure S5c). During the overnight period there were few passenger cars on the road. The fraction of CIVs dropped to 0.11 ± 0.027 during the morning rush hour (5:00 to 9:59

ET) and further declined to 0.073 ± 0.024 during the afternoon rush hour (14:00 – 20:59 ET). In terms of day-of-week, the fraction of CIVs decreased by a factor of 2 from 0.14 on weekdays to 0.074 on weekends (Table 2 and Figure S5f).

**Table 2.** Traffic composition of vehicles passing the I-95 NR traffic counter pre-COVID (April 2017 and 2018) and in April 2020 by weekday and local time. SIV represents spark-ignited vehicles and CIV indicates compression-ignited vehicles.

| | **April 2017 & 2018 SIV (CIV)** | **April 2020 SIV (CIV)** |
|---|---|---|
| **All Days and Hours** | 88% (12%) | 79% (21%) |
| **Weekdays Only (M-F)** | 86% (14%) | 77% (23%) |
| **Weekends Only (S-S)** | 93% (7%) | 84% (16%) |
| **Overnight Hours (23:00 – 4:59 AM Local)** | 78% (22%) | 63% (37%) |
| **Morning Rush Hours (5:00 – 9:59 AM Local)** | 89% (11%) | 82% (18%) |
| **Afternoon Rush Hours (14:00 – 20:59 Local)** | 93% (7%) | 88% (12%) |

The traffic composition passing the I-95 NR site in April 2020 exhibited higher fractions of CIVs for all time windows than in April of 2017 and 2018. In April 2020, the fleet consisted of 79% cars, motorcycles, and pick-up trucks; 0.010% buses; 4.9% single-unit trucks; and 16% tractor-trailer trucks (Table 2). The total number of on-road passenger cars declined much more than the number of trucks (Figure S5), resulting in a doubling of the fraction of CIVs relative to SIVs from 12% pre-COVID to 21% in April 2020 (Table 2).

While CIVs represent the minority of vehicles passing the NR site, their contribution to highway emissions of BC and $NO_x$ can be substantial. As demonstrated in a tunnel study by Dallmann et al. (2013), medium- and heavy-duty trucks, composing as little as <1% of the fleet, contributed up to 45% of BC and 18% of $NO_x$ concentrations. With the fraction of CIVs along I-95 increasing from 12% in April 2017 and 2018 to 21% in April 2020 (Table 2), diesel trucks would have had a greater contribution to mobile emissions in April 2020 than in prior years.

### 3.1.2 Influence of Pandemic-Related Travel Restrictions on Traffic Flow and Inferred Vehicular Emissions

Significant reductions in the number of on-road vehicles in April 2020 affected fleet composition, vehicle speed, and stop-and-go traffic. The weighted mean vehicle speed ($\mu$) on I-95 was 14% higher in April 2020 ($\mu$ = 30.3 m $s^{-1}$) compared to prior years ($\mu$ = 26.6 m $s^{-1}$) and the fraction of vehicles driving slower than 22 m $s^{-1}$ was nearly eliminated in April 2020 (Figure 2). The threshold of 22 m $s^{-1}$ was selected because the speed limit on this portion of the highway is 29 m $s^{-1}$ and speeds slower than 22 m $s^{-1}$ typically indicate traffic jams marked by more frequent braking and accelerating. Repeating this analysis by weekday and local time shows consistent results with higher speeds and virtually eradicated stop-and-go traffic in April 2020 relative to prior years (Table S3). The only time period with comparable mean vehicle speed and lack of traffic congestion between April 2020 and prior years was the overnight period (23:00 – 4:59 AM ET), marked by fewer on-road vehicles and little traffic congestion (Table S3).

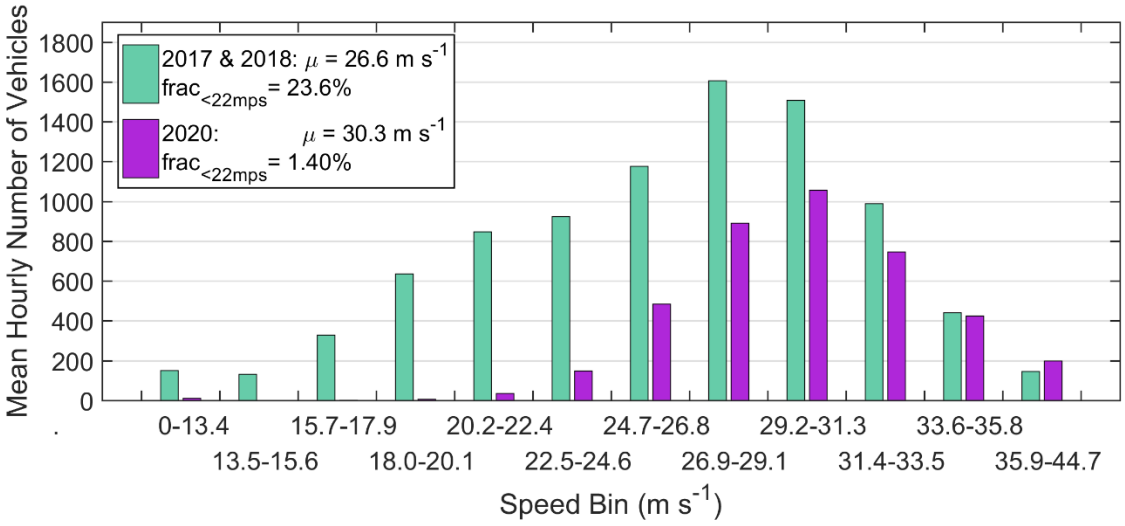


**Figure 2.** Mean hourly number of vehicles in each of 12 speed bins in April 2017 and 2018 (turquoise) and April 2020 (purple) at a traffic sensor located on I-95 in Howard County, MD. Provided in the top left-hand corner is the weighted mean speed and the fraction of vehicles driving slower than 22 m $s^{-1}$ ($frac_{<22mps}$) pre-COVID and in April 2020.

Fewer on-road vehicles in April 2020 resulted in reduced mobile emissions as well as lower ambient BC, CO, $NO_x$, and $CO_2$ mixing ratios compared to prior years at the I-95 NR site (Table S4). Rather than use absolute concentrations, affected by other processes including changing boundary layer height, here we use concentration ratios to infer emissions and to better understand the impact of fewer vehicle miles traveled and changing traffic patterns on the emission of pollutants.

A comparison of inferred emission ratios for April 2020 and pre-COVID by weekday and local time is presented in Table 3. The difference in temperature between April 2020 and prior Aprils was small (2.2 °C) and its impact on our temperature analysis is discussed in Section 3.2.1.

**Table 3.** Median inferred emission ratios for April 2017 & 2018 ("pre-COVID") and April 2020 ("2020") at the I-95 NR site. Also provided is the relative difference (%), with the statistical significance indicated by the p-value, between each pair of median values for each emission ratio and time period considered. Percentages of CIVs and SIVs provided are for typical pre-COVID traffic composition.

| | Temperature (°C) | ΔBC/ΔCO ($\mu g\ m^{-3}$) $(\mu g\ m^{-3})^{-1}$ | ΔBC/ΔCO$_2$ ($\mu g\ m^{-3}$) $(\mu g\ m^{-3})^{-1}$ | ΔNO$_x$/ΔCO ppbv ppbv$^{-1}$ | ΔCO/ΔCO$_2$ ppbv ppmv$^{-1}$ | ΔNO$_x$/ΔCO$_2$ ppbv ppmv$^{-1}$ |
|---|---|---|---|---|---|---|
| **All Days and Hours** | | **(Pre-COVID: 12% CIV, 88% SIV)** | | | | |
| Pre−COVID | 14.4 | 0.0104 | $5.11 \times 10^{-5}$ | 0.247 | 8.02 | 2.05 |
| 2020 | 12.2 | 0.0076 | $3.75 \times 10^{-5}$ | 0.276 | 8.40 | 2.37 |
| Relative | | **−26.9%** | **−26.6%** | 11.7% | 4.74% | **15.6%** |
| Change (%) | | **(p<0.05)** | **(p<0.05)** | (p = 0.074) | (p = 0.41) | **(p<0.05)** |
| **Weekdays Only** | | **(Pre-COVID: 14% CIV, 86% SIV)** | | | | |
| Pre−COVID | 13.9 | 0.0125 | $5.54 \times 10^{-5}$ | 0.282 | 7.69 | 2.21 |
| 2020 | 11.7 | 0.0096 | $4.23 \times 10^{-5}$ | 0.313 | 7.19 | 2.49 |
| Relative | | **−23.2%** | **−23.6%** | **11.0%** | −6.50% | **12.7%** |
| Change (%) | | **(p<0.05)** | **(p<0.05)** | **(p<0.05)** | (p = 0.26) | **(p<0.05)** |
| **Weekends Only** | | **(Pre-COVID: 7.4% CIV, 92.6% SIV)** | | | | |
| Pre−COVID | 15.3 | 0.0056 | $3.31 \times 10^{-5}$ | 0.159 | 9.09 | 1.41 |
| 2020 | 12.2 | 0.0038 | $2.76 \times 10^{-5}$ | 0.169 | 12.5 | 2.05 |
| Relative | | **−32.1%** | −16.6% | 6.29% | **37.5%** | **45.4%** |
| Change (%) | | **(p<0.05)** | (p = 0.27) | (p = 0.68) | **(p<0.05)** | **(p<0.05)** |
| **23:00 – 4:59 AM Local Time** | | **(Pre-COVID: 22% CIV, 78% SIV)** | | | | |
| Pre−COVID | 11.7 | 0.0151 | $6.39 \times 10^{-5}$ | 0.439 | 6.62 | 3.03 |
| 2020 | 10.0 | 0.0128 | $4.52 \times 10^{-5}$ | 0.549 | 5.26 | 2.94 |
| Relative | | −15.2% | **−29.3%** | **25.1%** | −20.5% | −2.97% |
| Change (%) | | (p = 0.12) | **(p<0.05)** | **(p<0.05)** | (p = 0.21) | (p = 0.76) |
| **5:00 – 9:59 AM Local Time** | | **(Pre-COVID: 11% CIV, 89% SIV)** | | | | |
| Pre−COVID | 11.7 | 0.0123 | $5.31 \times 10^{-5}$ | 0.280 | 7.63 | 1.96 |
| 2020 | 10.0 | 0.0095 | $3.94 \times 10^{-5}$ | 0.296 | 6.45 | 2.08 |
| Relative | | **−22.8%** | **−25.8%** | 5.71% | −15.5% | 6.12% |
| Change (%) | | **(p<0.05)** | **(p<0.05)** | (p = 0.17) | (p = 0.23) | (p = 0.76) |
| **14:00 – 20:59 Local Time** | | **(Pre-COVID: 7.3% CIV, 92.7% SIV)** | | | | |
| Pre−COVID | 18.3 | 0.0076 | $4.25 \times 10^{-5}$ | 0.189 | 8.93 | 1.63 |
| 2020 | 14.4 | 0.0038 | $3.04 \times 10^{-5}$ | 0.169 | 12.8 | 2.48 |
| Relative | | **−50.0** | **−28.5** | −10.6 | **43.3%** | **52.1%** |
| Change (%) | | **(p<0.05)** | **(p<0.05)** | (p = 0.12) | **(p<0.05)** | **(p<0.05)** |

Table 3 shows that ΔBC/ΔCO in April 2020 was 26.9% (p<0.05) lower than in prior years, considering all days and hours. Likewise, ΔBC/ΔCO$_2$ was 26.6% (p<0.05) lower in April

2020. With SIVs (i.e., passenger cars) exhibiting a much larger decline in numbers than CIVs (i.e., trucks) in 2020, one initial hypothesis was that the reduction in mobile CO and $CO_2$ emissions would be greater than that for BC and thus lead to an increase in $\Delta BC/\Delta CO$ and $\Delta BC/\Delta CO_2$ during April 2020. Instead, we observed consistently lower values of $\Delta BC/\Delta CO$ in April 2020 compared to prior years. The $\Delta BC/\Delta CO_2$ ratio exhibited a statistically significant decrease in all time periods except for weekends, which had a statistically insignificant decrease in the emission ratio. These findings indicate that the influence of vehicle fleet changes on $\Delta BC/\Delta CO$ and $\Delta BC/\Delta CO_2$ was overshadowed by a drastic change in another highway characteristic: stop-and-go traffic.

While the differences in mean traffic speeds were generally minor (<6 m $s^{-1}$), the fraction of vehicles driving below 22 m $s^{-1}$ ($frac_{<22mps}$) dropped down from 23.6% in prior years to less than 2% in April 2020 (Figure 2 and Table S3). The afternoon rush hour (14:00 – 20:59 ET), when the $frac_{<22mps}$ was highest of the day at 35.4% (Table S3), exhibited the largest decrease in $\Delta BC/\Delta CO$ (−50.0%, $p<0.05$) from April 2017 and 2018 to April 2020 (Table 3). The morning rush hour also saw a significant improvement in traffic flow, with the percentage of vehicles driving slower than 22 m $s^{-1}$ decreasing from 24.1% pre-COVID to 1.23% in April 2020, and a concurrent decrease of 22.8% in $\Delta BC/\Delta CO$ and 25.8% in $\Delta BC/\Delta CO_2$ (Table 3). The drop in $\Delta BC/\Delta CO$ during the overnight period (23:00 – 4:59 ET), when traffic flow did not differ much in April 2020 compared to previous years, was less remarkable and statistically insignificant (−15.2%, $p = 0.12$).

The difference in $\Delta BC/\Delta CO$ and $\Delta BC/\Delta CO_2$ between weekdays and weekends suggests that CIVs are the primary contributor to mobile BC emissions at the I-95 NR site. The median pre-COVID $\Delta BC/\Delta CO$ ratio on weekdays was 0.0125 compared to the weekend ratio of 0.0056,

342 a decrease of 55.2% (Table 3). Similarly, $\Delta BC/\Delta CO_2$ decreased by 40.3% from $5.54 \times 10^{-5}$ on
343 weekdays to $3.31 \times 10^{-5}$ on weekends. Note that for both $\Delta BC/\Delta CO$ and $\Delta BC/\Delta CO_2$, the units
344 of $\Delta BC$, $\Delta CO$, and $\Delta CO_2$ ($\mu g\ m^{-3}$) are the same and hence the ratios are expressed as unitless
345 quantities but are mass ratios. The decrease in both ratios from weekdays to weekends followed
346 the change in the fraction of CIVs passing the NR site: the fraction of CIVs dropped from 14%
347 on weekdays to 7.4% on weekends, resulting in a decrease of 47.1% (Table 2). These
348 observations provide strong evidence that CIVs dominate the BC emissions at the I-95 NR site.

349 Figure 2 shows that traffic congestion was nearly eradicated in April 2020. Two
350 mechanisms may help to explain the decline in $\Delta BC/\Delta CO$ and $\Delta BC/\Delta CO_2$ during the time of
351 little to no stop-and-go traffic: BC emissions from brake pad wear and acceleration in CIVs.
352 Vehicular brake pads, composed of various metals and graphite, are known to emit BC and a
353 variety of other species (Lyu & Olofsson, 2020). Significant alleviation of stop-and-go traffic in
354 April 2020 thus led to lower BC emissions from brake pad wear. Black carbon is also released
355 from the exhaust of CIVs during acceleration (Giakoumis & Zachiotis, 2021; Rakopoulos &
356 Giakoumis, 2009), and emissions from tailpipes are expected to be higher than those from brake
357 pad wear in the NR environment. With CIVs representing the dominant source of exhaust
358 emissions of BC, the near-elimination of traffic jams in April 2020 produced a larger reduction
359 in mobile BC emissions than the effect of fewer on-road SIVs on CO emissions. Given a
360 decrease in the number of SIVs of 60% in April 2020 and assuming a comparable reduction in
361 CO emissions, the decrease in $\Delta BC/\Delta CO$ of 26.7% (considering all days and hours) indicates
362 that BC emissions likely decreased by up to 70%, a number compatible with the decrease in the
363 median BC concentration of nearly a factor of two (Table S4).

Table 3 presents the results for various other emission ratios; comparison of CO and $NO_x$ to $CO_2$ provides better understanding of the effectiveness of exhaust-aftertreatment devices, specifically catalytic converters, installed in vehicles passing the NR site. Trucks generally emit less CO relative to $CO_2$, resulting in lower $\Delta CO/\Delta CO_2$ than cars (Figure S6). With fewer on-road SIVs relative to CIVs in April 2020, one might expect lower $\Delta CO/\Delta CO_2$ as well. The $\Delta CO/\Delta CO_2$ analysis presented in Table 3 shows no significant effect considering all hours; however, we observe higher ratios on weekends and during the afternoon rush hour in April 2020 than in previous years. A plausible explanation for this observation is that vehicles emit more CO at high speeds (Hickman et al., 1999; OECD & ECMT, 2006; Wang et al., 2018; Figure S7). With less traffic congestion on I-95 in April 2020, vehicles were driving 14% faster than usual (Figure 2) and emitted more CO relative to $CO_2$.

A statistically significant increase in $\Delta NO_x/\Delta CO_2$ was observed for weekdays, weekends, and during the afternoon rush hour. $\Delta NO_x/\Delta CO_2$ increased by 45.4% ($p<0.05$) on weekends and 52.1% ($p<0.05$) in the afternoon rush hours, compared to 12.7% on weekdays (Table 3). The increase in $\Delta NO_x/\Delta CO_2$ can be explained by elevated $NO_x$ emissions from SIVs at high speeds, as well as the higher fraction of CIVs in April 2020 than in April 2017 and 2018. Since the $\Delta NO_x/\Delta CO_2$ emission ratio from CIVs is approximately ten times higher than from SIVs (O'Driscoll et al., 2018), a greater fraction of on-road CIVs in April 2020 would have led to elevated $\Delta NO_x/\Delta CO_2$ (but lower $NO_x$ mixing ratios; Table S4) for all days and hours in April 2020 compared to April 2017 and 2018. The time periods that had the largest increase in $\Delta NO_x/\Delta CO_2$ (weekends and the afternoon rush hours) also had the highest fraction of SIVs compared to weekdays, overnight, and the morning rush hours, both in April 2020 and April of prior years. A plausible explanation for this finding is that gasoline vehicles emit more $NO_x$ at

high speeds (Kean et al., 2003; OECD & ECMT, 2006), contributing to the higher $\Delta NO_x/\Delta CO_2$ observed at times when the fraction of SIV was at a maximum in April 2020. Figure S8 shows a strong dependence of MOVES-estimated $NO_x$ emission factors (per distance traveled) on vehicle speeds; $NO_x$ emission factors from MOVES were 28% higher for SIVs traveling at speeds faster than 32.4 m $s^{-1}$ than for those driving at 22.4 m $s^{-1}$ (Figure S8). In April of 2017 and 2018, 12% of the I-95 vehicle fleet drove faster than 32.4 m $s^{-1}$, while in April of 2020 this fraction increased to 25% of the vehicle fleet. The shift toward faster speeds would have led to greater speed-related $NO_x$ emissions from SIVs in April 2020 than in April 2017 and 2018 and contributed to the observed increase in $\Delta NO_x/\Delta CO_2$. With CO emissions from SIVs also increasing with higher speeds (Figure S7), a likely explanation for the increase in $\Delta CO/\Delta CO_2$ from April 2017 and 2018 to April 2020 on weekends and during the afternoon rush hours is similar to that discussed for $NO_x$ emissions.

To evaluate the sensitivity of the results presented in Table 3, we repeated the analysis using a different method of estimating emission ratios, as well as for August 2020 when on-road traffic had increased. To test the impact of the method used to estimate emission ratios, we repeated the analysis using a background subtraction technique similar to that discussed in Brantley et al. (2014). The details of how background concentrations were calculated are provided in Section S2 of the SI. The results, shown in Table S7, are similar to those in Table 3 and do not change our conclusions. Differences in vehicle speeds, SIV/CIV fleet composition, and frequency of stop-and-go traffic between August 2020 and August 2017/2018 were smaller compared to differences between April 2020 and April 2017/2018 (Tables S8 and S9). More on-road vehicles in August 2020 than in April 2020 led to more frequent traffic congestion, resulting

409 in less significant decreases in $\Delta BC/\Delta CO$ and $\Delta BC/\Delta CO_2$, as well as smaller increases in

410 $\Delta NO_x/\Delta CO_2$ and $\Delta CO/\Delta CO_2$ in August than in April (Table S10).

411

412 **3.2. Temperature Sensitivity of Vehicular BC Emissions**

413 **3.2.1. Near-Road Ambient Observations**

414

415 Previous studies reported a seasonal cycle in observed $\Delta BC/\Delta CO$ at suburban and urban

416 sites, with higher $\Delta BC/\Delta CO$ emission ratios in the summer than in the winter (Chen et al., 2001;

417 Kondo et al., 2006). Additionally, Wang et al. (2018) found higher BC fuel-based emission

418 factors ($mg_{BC}\ kg^{-1}{}_{fuel}$) in the spring-summer than in the fall-winter using observations collected

419 adjacent to a four-lane highway in Toronto, Canada. A similar seasonal pattern is evident at the

420 I-95 NR site. Figure 3 shows seasonal mean values of $\Delta BC/\Delta CO$ ratios for 2017 and 2018

421 separately (colored by season) and 2017-2018 combined (filled black circles) as a function of

422 ambient temperature. At the I-95 NR site, the highest $\Delta BC/\Delta CO$ ratio occurred in summer and

423 lowest $\Delta BC/\Delta CO$ in winter. Seasonal mean $\Delta BC/\Delta CO$, calculated from the hourly emission

424 ratios, were strongly correlated with ambient temperature ($r^2 = 0.96$) and increased by 81% from

425 winter (5 °C) to summer (25 °C). The seasonal changes in $\Delta BC/\Delta CO$ and proximity of the NR

426 site to a major highway suggests a temperature sensitivity in vehicular emissions, particularly

427 those from diesel trucks.

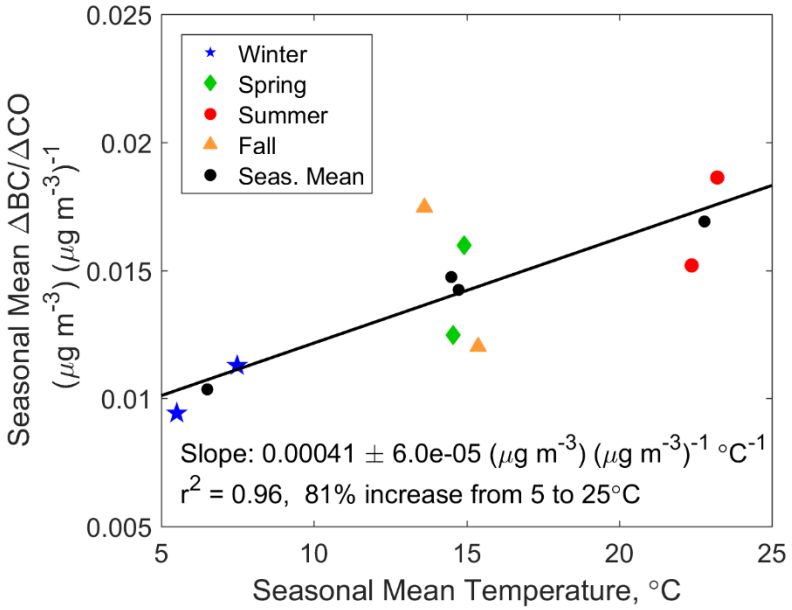


**Figure 3.** Seasonal variability in ΔBC/ΔCO inferred from observations collected at the I-95 NR site from January 2017 through December 2018. Each season contains two colored symbols for 2017 and 2018 separately, with the mean of the two shown by the filled black circles. Blue stars represent winter (December – February), green diamonds represent spring (March – May), red circles represent summer (June – August), and orange triangles represent fall (September – November). The mean emission ratio in each season is represented by the filled black circles, fitted using a linear geometric mean regression (solid black line) with regression statistics provided on the bottom of the plot.

To avoid potential impacts of seasonal fuel switching on emissions, we focus on the temperature dependence of ΔBC/ΔCO during the cold season. Figure 4 shows that ΔBC/ΔCO and $\Delta BC/\Delta CO_2$ exhibit a positive correlation with ambient temperature considering all hours and days of the week during the cold months, defined as November, December, January, and February, in 2017 and 2018. Hourly ΔBC/ΔCO and $\Delta BC/\Delta CO_2$ were placed into ten equal-numbered bins, sorted by ascending temperature. Figure 4 shows the median and 25$^{th}$ and 75$^{th}$ percentile values for each of these temperature bins, along with an ordinary linear least-squares regression fit to the median values. Considering all data, both emission ratios exhibited a statistically significant increase with temperature: $1.4 \pm 0.40 \times 10^{-4}$ °C$^{-1}$ in ΔBC/ΔCO and $1.0 \pm 0.27 \times 10^{-6}$ °C$^{-1}$ in $\Delta BC/\Delta CO_2$, equivalent to an increase of 56% in ΔBC/ΔCO and 83% in

447 $\Delta BC/\Delta CO_2$ from −5 °C to 20 °C (Figure 4). Using these regression parameters, the difference in
448 temperature between April 2020 relative to the April of prior years (April 2020 was 2.2 °C
449 cooler) can only account for a 3-4% decrease in the $\Delta BC/\Delta CO$ and $\Delta BC/\Delta CO_2$ quantified in
450 Table 3. Similar temperature sensitivities were obtained when hourly emission ratios were
451 calculated with an orthogonal linear regression instead of geometric mean regression. Repeating
452 the analysis in Figure 4 for the upwind region of the NR site (225 to 360 °) results in statistically
453 insignificant changes in both $\Delta BC/\Delta CO$ and $\Delta BC/\Delta CO_2$ with temperature (Figure S10). The
454 absence of a temperature effect in the upwind region supports the finding of Figure 4 that direct
455 vehicular emissions are sensitive to ambient temperature.

456

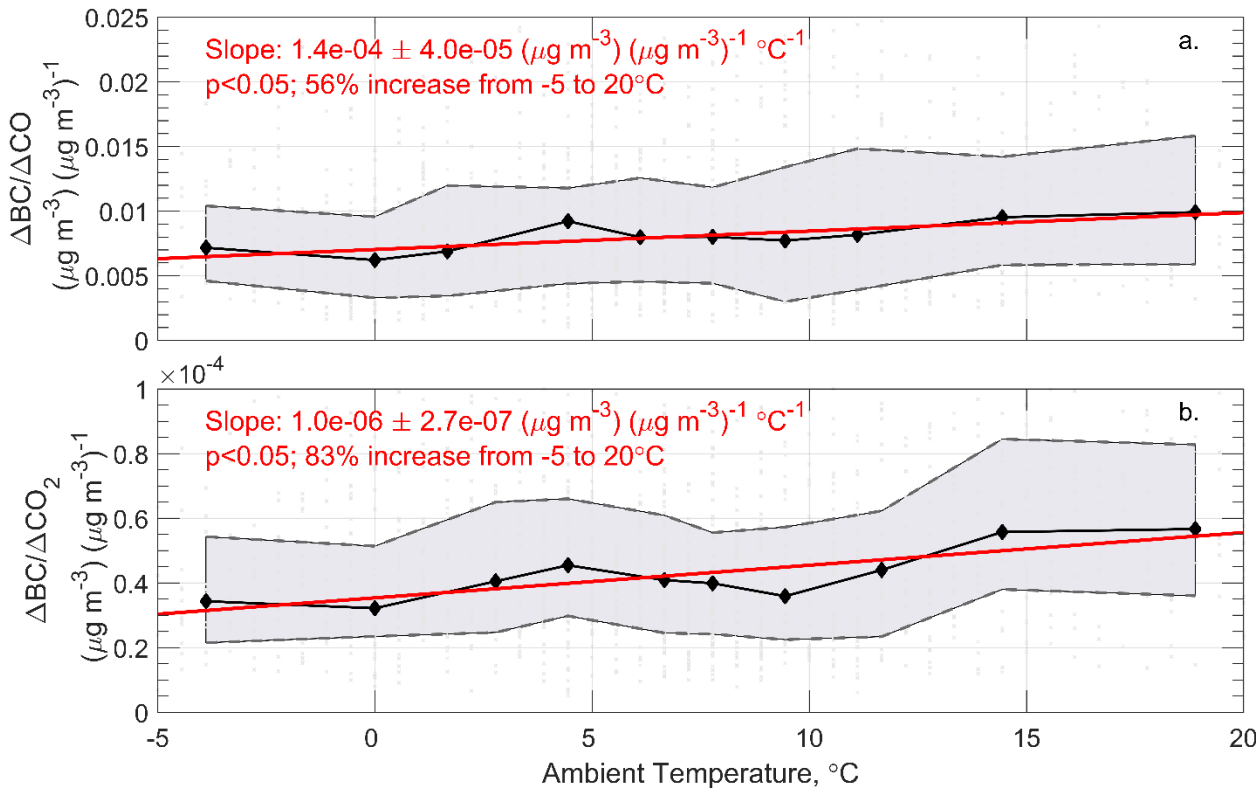


457

458 **Figure 4.** Hourly $\Delta BC/\Delta CO$ (a) and $\Delta BC/\Delta CO_2$ (b) inferred from I-95 NR observations as a function of
459 ambient temperature for the cold season in 2017 and 2018. Hourly ratios (light gray points) were
460 estimated from the slope values of linear geometric mean regressions (±standard error) performed on five-
461 minute mean data within each hour. Only hours with winds originating from the highway were included

462 in the analysis. Hourly data were compiled into ten equal-sized bins, with the median value of each bin
463 represented by the black diamonds, and the 25$^{th}$ and 75$^{th}$ percentile values by the dashed black line. An
464 ordinary least-squares regression was fit to the binned median values (red line) and the details of the
465 regression provided in the top left of each plot. The statistical significance of each regression was
466 determined by the non-parametric Mann-Kendall test (Gilbert, 1987; Kendall, 1975; Mann, 1945).

467

468 As shown previously, vehicular running emissions of CO and $CO_2$ do not appear
469 sensitive to temperature during the cold season (Hall et al., 2020). Thus, the increase in
470 $\Delta BC/\Delta CO$ and $\Delta BC/\Delta CO_2$ is likely due to an increase in BC emissions from mobile sources at
471 higher temperatures. Some evidence suggests that gasoline vehicles utilizing direct injection and
472 particulate filters appear to remove BC more efficiently at lower intake temperatures (Chan et al.,
473 2013). Direct injection, the mechanism in diesel engines, may also be employed with gasoline
474 engines and has been on the rise in recent years (US EPA, 2020b) to provide more power and
475 increase fuel efficiency. Like in diesel engines, this mechanism of injecting fuel directly into the
476 cylinder produces more BC emissions. However, diesel engines emit the vast majority of BC
477 reaching the NR site and thus a more plausible explanation for the temperature sensitivity lies
478 within diesel vehicles. Turbochargers on diesel engines compress intake air, leading to higher
479 temperatures and lower densities. This can favor elevated BC production as the air-to-fuel ratio
480 is reduced (Chen et al., 2001; Ghazikhani et al., 2013). Diesel trucks equipped with
481 turbochargers typically also utilize charge-air coolers, or turbo coolers. In an air-to-air turbo
482 cooler, the hot, compressed air is cooled via heat exchange with outside air (Joshi et al., 2009;
483 Sher, 1998), resulting in greater air density and lower emissions of $NO_x$ and BC (Cipollone et al.,
484 2017). Because compressed air is cooled by heat exchange with ambient air, and also because
485 the coolers degrade over time (Joshi et al., 2009), higher ambient temperatures may lead to less
486 cooling of the intake air and, in turn, higher BC emissions at warmer conditions. This process

487 can lead to increasing BC emissions, and higher $\Delta BC/\Delta CO$ and $\Delta BC/\Delta CO_2$, with rising
488 temperature, as observed in Figure 4.

489 To further explore the contribution of the vehicle fleet composition on the temperature
490 sensitivity, we repeated the analysis by day of week and at different times of the day. Both
491 $\Delta BC/\Delta CO$ and $\Delta BC/\Delta CO_2$ exhibited a significant increase with rising temperature on weekdays
492 ($p<0.05$) absent on weekends (Table 4). Both the total truck traffic (1,022 vehicles/hr on weekdays
493 and 433 vehicles/hr on weekends) and the fraction of CIVs (14% on weekdays and 7.4% on
494 weekends) dropped by a factor of two from weekdays to weekends. Traffic congestion marked by
495 slow-moving vehicles ($< 22$ m $s^{-1}$) was greater on weekdays (24%) than on weekends (11%, Table
496 S3), resulting in higher weekday BC emissions from diesel trucks due to the stop-and-go effect
497 discussed in Section 3.1.2. With diesel trucks emitting the bulk of on-road BC emissions, the
498 increase in $\Delta BC/\Delta CO$ and $\Delta BC/\Delta CO_2$ with rising temperature on weekdays suggests that the
499 emission of BC from diesel vehicles is sensitive to ambient temperature.

500

501

502

503

504

505

506

**Table 4.** Measured $\Delta BC/\Delta CO$ and $\Delta BC/\Delta CO_2$ as a function of ambient temperature during the months of November, December, January, and February in 2017 and 2018 at the I-95 NR site. Hourly emission ratios were placed into ten equal-sized bins and an ordinary linear regression fit to the median emission ratios of each bin, the same as in Figure 4.

| | I−95 Fleet CIV / SIV | $(\Delta BC/\Delta CO) / T$ $(\mu g\ m^{-3})\ (\mu g\ m^{-3})^{-1}\ °C^{-1}$ | $(\Delta BC/\Delta CO_2) / T$ $(\mu g\ m^{-3})\ (\mu g\ m^{-3})^{-1}\ °C^{-1}$ |
|---|---|---|---|
| All Days and Hours | 12% / 88% | **$1.42\ (\pm 0.40) \times 10^{-4}$ (p<0.05)** | **$1.01\ (\pm 0.27) \times 10^{-6}$ (p<0.05)** |
| Weekdays Only | 14% / 86% | **$1.64\ (\pm 0.68) \times 10^{-4}$ (p<0.05)** | **$1.06\ (\pm 0.19) \times 10^{-6}$ (p<0.05)** |
| Weekends Only | 7.4% / 92.6% | $-0.085\ (\pm 0.06) \times 10^{-4}$ (p = 0.72) | $0.072\ (\pm 0.24) \times 10^{-6}$ (p = 1) |
| Overnight (23:00 – 4:59 AM ET) | 22% / 78% | **$2.84\ (\pm 0.84) \times 10^{-4}$ (p<0.05)** | **$0.96\ (\pm 0.58) \times 10^{-6}$ (p<0.05)** |
| Morning Rush Hours (5:00 – 9:59 AM ET) | 11% / 89% | **$3.62\ (\pm 0.83) \times 10^{-4}$ (p<0.05)** | **$1.48\ (\pm 0.32) \times 10^{-6}$ (p<0.05)** |
| Afternoon Rush Hours (14:00 – 20:59 ET) | 7.3% / 92.7% | **$1.59\ (\pm 0.43) \times 10^{-4}$ (p<0.05)** | $1.00\ (\pm 1.48) \times 10^{-6}$ (p = 0.074) |

A positive correlation between $\Delta BC/\Delta CO$ and temperature was evident in all three local time windows (Table 4). The slope with temperature ($°C^{-1}$) was highest during the morning rush hours [$3.62\ (\pm 0.83) \times 10^{-4}$, $p<0.05$], followed by the overnight period [$2.84\ (\pm 0.84) \times 10^{-4}$, $p<0.05$], and was lowest in the afternoon rush hours [$1.59\ (\pm 0.43) \times 10^{-4}$, $p<0.05$]. These results indicate that fleet make-up and driving conditions both contribute to BC emissions.

Patterns in the temperature dependence of $\Delta BC/\Delta CO$ by local time follow the fraction of CIVs and vehicular traffic over the course of the day. The overnight period experienced the highest fraction of CIVs to total vehicles, even though the total number of trucks on the road was lower than during the rest of the day (Figure S5). The temperature dependence in BC emissions

observed in the overnight period was likely driven by the high fraction (22%) of diesel vehicles (Table 4).

The morning rush hour exhibited the largest slopes of $\Delta BC/\Delta CO$ and $\Delta BC/\Delta CO_2$ with temperature. While the fraction of CIVs to total vehicles in the morning (11%) was lower than overnight (22%), stop-and-go traffic was more common during the morning rush hour than during the overnight period (Table S3). A plausible explanation for the observed temperature sensitivity in the morning is that elevated BC emissions from CIVs due to frequent acceleration enhances the temperature effect from diesel engines.

The temperature sensitivity of $\Delta BC/\Delta CO$ in the afternoon rush hours had the lowest slope considering all times of day [1.59 (± 0.43) $\times 10^{-4}$ °$C^{-1}$, $p<0.05$] (Table 4). The slope of $\Delta BC/\Delta CO_2$ was also at a minimum in the afternoon rush hours, but the regression was statistically significant only at the 90% confidence level ($p = 0.074$). Given that CIVs make up only 7.3% of the vehicles passing the I-95 NR site in the afternoon, the sensitivity in $\Delta BC/\Delta CO$ likely originates from high BC emissions by CIVs due to a peak in stop-and-go traffic during the afternoon rush hour or a combination of CIV and SIV.

### 3.2.2. MOVES Simulations

Here we compare the $\Delta BC/\Delta CO$ and $\Delta BC/\Delta CO_2$ temperature sensitivity in mobile emissions inferred at the I-95 NR site to MOVES3 output. MOVES3 was run using 2017 input data, the latest year with available data, supplied by the Maryland Department of the Environment for Howard County, MD, the county in which the I-95 NR site resides. Data used

543 as input for the model include average speed distribution, meteorology, road type distribution,
544 fuel information, and vehicle age, populations, and miles traveled by hour, weekday, and month.

545 Unlike prior versions, MOVES3 does not adjust hot-running exhaust of $PM_{2.5}$ from any
546 gasoline or diesel vehicle for ambient temperature. The temperature adjustment for gasoline
547 vehicles of MY 2004 and earlier was removed in the development of MOVES3 (US EPA, 2020a;
548 Table S6). Figure 5 documents the lack of sensitivity; the temperature dependence simulated by
549 MOVES in the I-95 weighted mean from −5 °C to 20 °C is negligible for both $\Delta BC/\Delta CO$
550 (0.04%) and $\Delta BC/\Delta CO_2$ (0.02%) and arises because of a small indirect adjustment to CO and
551 $CO_2$ emissions due to increased air conditioner use at higher temperatures that exists in both
552 MOVES3 and MOVES2014 (Hall et al., 2020; US EPA, 2020a). The absence of a temperature
553 effect is robust regardless of vehicle type and fuel use. Negating the temperature adjustment
554 factors for hot-running emissions does not appear to represent conditions along I-95 well: the
555 observed increase in emission ratios from −5 to 20 °C at the I-95 NR site, considering all
556 weekdays and hours of the day, was 56% in $\Delta BC/\Delta CO$ and 83% in $\Delta BC/\Delta CO_2$ (Figure 4). With
557 the air conditioning effect at a minimum in the observed temperature range and inferred mobile
558 emissions of CO and $CO_2$ at the NR site exhibiting an insignificant temperature impact (Hall et
559 al., 2020), the temperature effects seen in $\Delta BC/\Delta CO$ and $\Delta BC/\Delta CO_2$ are likely the result of an
560 increase in BC emissions with rising temperatures that is not represented within MOVES as
561 configured.

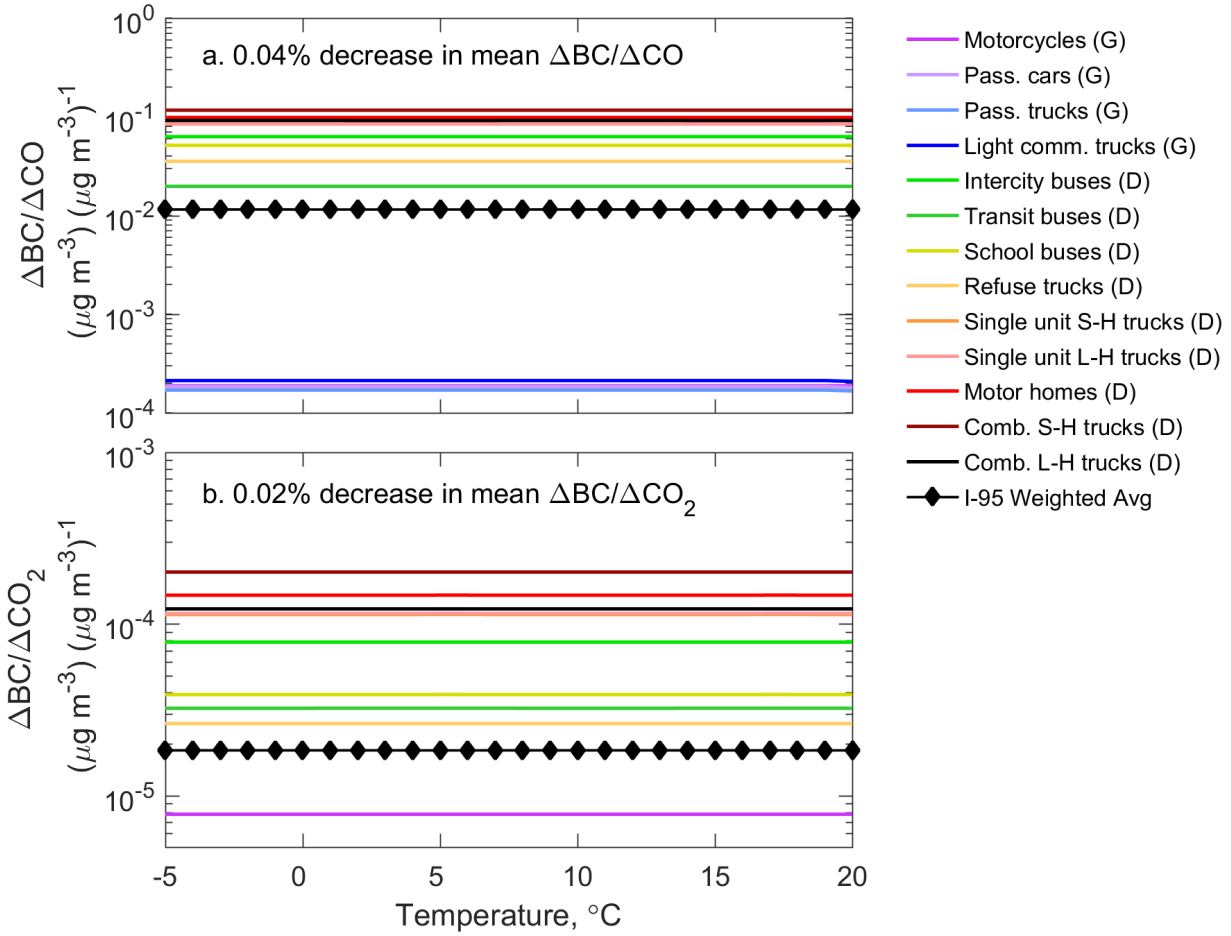


**Figure 4.** MOVES3 simulated ΔBC/ΔCO and ΔBC/Δ$CO_2$ as a function of temperature for the 13 different vehicle types modeled in MOVES. The dominant type of fuel (G for gasoline and D for diesel) is provided next to each vehicle type and is based on county-level data compiled by the Maryland Department of the Environment mobile emissions team. The weighted mean emission ratios were calculated using the fractions of various vehicle types derived from traffic counts collected at the traffic counter site along I-95. S-H indicates short-haul while L-H represents long-haul combination unit trucks.

## 4. Conclusions

Peak travel restrictions at the beginning of the COVID-19 pandemic in April 2020 enabled us to quantify the effects of traffic flow on BC emissions from diesel trucks. Lower ΔBC/ΔCO and ΔBC/Δ$CO_2$ observed in April 2020 compared to prior years likely resulted from diesel trucks emitting far less BC in 2020 than under typical, congested traffic conditions with

frequent acceleration. These results suggest that eliminating traffic jams could reduce highway BC emissions from diesel trucks by up to 70% (i.e., to 30% of normal BC emissions). Similar reductions in mobile BC emissions may be possible with diesel engine designs that reduce turbocharger lag.

Vehicular BC emissions are observed to exhibit a strong sensitivity to ambient temperature. Prior to COVID restrictions we observed a 56% increase in $\Delta BC/\Delta CO$ as temperature rose from −5 to 20 °C. The overnight period, when the fraction of CIVs was at a maximum, had a strong increase in $\Delta BC/\Delta CO$ and $\Delta BC/\Delta CO_2$ with temperature, suggesting BC emissions from diesel trucks are sensitive to temperature. The observed sensitivity may result from emissions control devices used on diesel engines producing elevated BC emissions at either warmer ambient conditions and/or lower air density.

Finally, the default settings of MOVES3 do not adjust for the temperature sensitivity of BC emissions, for any type of vehicle. Future air quality simulations would benefit from incorporation of a realistic temperature dependence of BC emissions within the default settings of this model. The future improvement of air quality model representation of BC emissions as a function of traffic patterns and possibly turbocharger lag is needed to improve the accuracy of air quality simulations from on-road vehicles, and to properly guide emissions engineering and public health policies.

**Acknowledgements**

We want to thank the Maryland Department of the Environment for support of the Regional Atmospheric Measurement Modeling and Prediction Program (RAMMPP; Grant

#U00P0600702), the National Institute of Standards and Technology (Grant #70NANB19H037) and the National Oceanic and Atmospheric Administration for support of greenhouse gas observations, and the EPA AQS program for the near-road measurements. We also want to thank Barry Balzanna, Abhay Nigam, and their team at the MD State Highway Administration for traffic observations; Joel Dreessen, Ryan Auvil, Aaron Ryan, and David Krask for their help with the NR observations; and Mohamed Khan and the MOVES team at MDE for providing input data and assistance with our MOVES3 simulations.

**Supporting Information** Includes Figures S1–S10 and Tables S1-S10 as referenced in text.

## References

Ahn, D. Y., Salawitch, R. J., Canty, T. P., He, H., Ren, X. R., Goldberg, D. L., & Dickerson, R. R. (2022). The U.S. power sector emissions of $CO_2$ and $NO_x$ during 2020: Separating the impact of the COVID-19 lockdowns from the weather and decreasing coal in fuel-mix profile. *Atmospheric Environment: X*, *14*, 100168. https://doi.org/https://doi.org/10.1016/j.aeaoa.2022.100168

Anderson, D. C., Loughner, C. P., Diskin, G., Weinheimer, A., Canty, T. P., Salawitch, R. J., Worden, H. M., Fried, A., Mikoviny, T., Wisthaler, A., & Dickerson, R. R. (2014). Measured and modeled CO and $NO_y$ in DISCOVER-AQ: An evaluation of emissions and chemistry over the eastern US. *Atmospheric Environment*, *96*, 78–87. https://doi.org/10.1016/j.atmosenv.2014.07.004

Appel, W. K., Bhave, P. V., Gilliland, A. B., Sarwar, G., & Roselle, S. J. (2008). Evaluation of the community multiscale air quality (CMAQ) model version 4.5: Sensitivities impacting model performance; Part II-particulate matter. *Atmospheric Environment*, *42*(24), 6057–

6066. https://doi.org/10.1016/j.atmosenv.2008.03.036

Ban-Weiss, G. A., McLaughlin, J. P., Harley, R. A., Lunden, M. M., Kirchstetter, T. W., Kean, A. J., Strawa, A. W., Stevenson, E. D., & Kendall, G. R. (2008). Long-term changes in emissions of nitrogen oxides and particulate matter from on-road gasoline and diesel vehicles. *Atmospheric Environment*, *42*(2), 220–232. https://doi.org/https://doi.org/10.1016/j.atmosenv.2007.09.049

Batterman, S. A., Zhang, K., & Kononowech, R. (2010). Prediction and analysis of near-road concentrations using a reduced-form emission/dispersion model. *Environmental Health*, *9*(1). https://doi.org/10.1186/1476-069X-9-29

Bishop, G. A., Haugen, M. J., McDonald, B. C., & Boies, A. M. (2022). Utah Wintertime Measurements of Heavy-Duty Vehicle Nitrogen Oxide Emission Factors. *Environmental Science & Technology*, *56*(3), 1885–1893. https://doi.org/10.1021/acs.est.1c06428

Book, E. K., Snow, R., Long, T., Fang, T., & Baldauf, R. (2015). Temperature effects on particulate emissions from DPF-equipped diesel trucks operating on conventional and biodiesel fuels. *Journal of the Air & Waste Management Association*, *65*(6), 751–758. https://doi.org/10.1080/10962247.2014.984817

Brantley, H. L., Hagler, G. S. W., Kimbrough, E. S., Williams, R. W., Mukerjee, S., & Neas, L. M. (2014). Mobile air monitoring data-processing strategies and effects on spatial air pollution trends. *Atmospheric Measurement Techniques*, *7*(7), 2169–2183. https://doi.org/10.5194/amt-7-2169-2014

Bureau of Transportation Statistics. (2018). *Estimated National Average Vehicle Emissions Rates per Vehicle by Vehicle Type Using Gasoline and Diesel*.

641 https://www.bts.gov/content/estimated-national-average-vehicle-emissions-rates-vehicle-
642 vehicle-type-using-gasoline-and

643 Chan, T. W., Meloche, E., Kubsh, J., Brezny, R., Rosenblatt, D., & Rideout, G. (2013). Impact
644 of ambient temperature on gaseous and particle emissions from a direct injection gasoline
645 vehicle and its implications on particle filtration. *SAE Technical Papers*, *2*(2), 350–371.
646 https://doi.org/10.4271/2013-01-0527

647 Chen, A. L.-W., Doddridge, B., Dickerson, R., Chow, J., Mueller, P., Quinn, J., & Butler, W.
648 (2001). Seasonal variations in elemental carbon aerosol, carbon monoxide and sulfur
649 dioxide: Implications for sources. *Geophysical Research Letters*, *28*(9), 1711–1714.

650 Cipollone, R., Di Battista, D., & Vittorini, D. (2017). Experimental assessment of engine charge
651 air cooling by a refrigeration unit. *Energy Procedia*, *126*, 1067–1074.
652 https://doi.org/https://doi.org/10.1016/j.egypro.2017.08.226

653 Crutzen, P. (1973). A discussion of the chemistry of some minor constituents in the stratosphere
654 and troposphere. *Pure and Applied Geophysics*, *106*, 1385–1399.
655 https://doi.org/10.1007/BF00881092

656 Dallmann, T. R., Kirchstetter, T. W., DeMartini, S. J., & Harley, R. A. (2013). Quantifying On-
657 Road Emissions from Gasoline-Powered Motor Vehicles: Accounting for the Presence of
658 Medium- and Heavy-Duty Diesel Trucks. *Environmental Science & Technology*, *47*(23),
659 13873–13881. https://doi.org/10.1021/es402875u

660 Dixit, P., Miller, J. W., Cocker, D. R., Oshinuga, A., Jiang, Y., Durbin, T. D., & Johnson, K. C.
661 (2017). Differences between emissions measured in urban driving and certification testing
662 of heavy-duty diesel engines. *Atmospheric Environment*, *166*, 276–285.

https://doi.org/10.1016/j.atmosenv.2017.06.037

Du, J., Rakha, H. A., Filali, F., & Eldardiry, H. (2021). COVID-19 pandemic impacts on traffic system delay, fuel consumption and emissions. *International Journal of Transportation Science and Technology*, *10*(2), 184–196. https://doi.org/https://doi.org/10.1016/j.ijtst.2020.11.003

Durbin, T. D., Johnson, K., Miller, J. W., Maldonado, H., & Chernich, D. (2008). Emissions from heavy-duty vehicles under actual on-road driving conditions. *Atmospheric Environment*, *42*(20), 4812–4821. https://doi.org/https://doi.org/10.1016/j.atmosenv.2008.02.006

Gaubert, B., Bouarar, I., Doumbia, T., Liu, Y., Stavrakou, T., Deroubaix, A., Darras, S., Elguindi, N., Granier, C., Lacey, F., Müller, J.-F., Shi, X., Tilmes, S., Wang, T., & Brasseur, G. P. (2021). Global Changes in Secondary Atmospheric Pollutants During the 2020 COVID-19 Pandemic. *Journal of Geophysical Research: Atmospheres*, *126*(8), e2020JD034213. https://doi.org/https://doi.org/10.1029/2020JD034213

Ghazikhani, M., Ebrahim, M., Mahian, O., & Sabazadeh, A. (2013). *Effects of Altitude on the Soot Emission and Fuel Consumption of a Light-Duty Diesel Engine*. *28*(2). https://doi.org/10.3846/16484142.2013.798743

Giakoumis, E. G., & Zachiotis, A. T. (2021). A comprehensive comparative investigation of a heavy-duty vehicle's performance, consumption and emissions during eight driving cycles. *International Journal of Ambient Energy*, *42*(1), 29–45. https://doi.org/10.1080/01430750.2018.1525578

Grange, S. K., Farren, N. J., Vaughan, A. R., Rose, R. A., & Carslaw, D. C. (2019). Strong

685 Temperature Dependence for Light-Duty Diesel Vehicle NOx Emissions. *Environmental*
686 *Science & Technology*, *53*, 6587–6596. https://doi.org/10.1021/acs.est.9b01024

687 Grieshop, A., Lipsky, E., Pekney, N., Takahama, S., & Robinson, A. (2006). Fine particle
688 emission factors from vehicles in a highway tunnel: Effects of fleet composition and season.
689 *Atmospheric Environment*, *40*, 287–298. https://doi.org/10.1016/j.atmosenv.2006.03.064

690 Grimes, C. D., & Dickerson, R. R. (2021). Evaluation of a filter-based black carbon (BC)
691 instrument using a brown carbon (BrC) surrogate as well as pure and coated BC surrogates.
692 *Aerosol Science and Technology*, *55*(5), 501–511.
693 https://doi.org/10.1080/02786826.2021.1878096

694 Hall, D. L., Anderson, D. C., Martin, C. R., Ren, X., Salawitch, R. J., He, H., Canty, T. P., Hains,
695 J. C., & Dickerson, R. R. (2020). Using near-road observations of CO, $NO_y$, and $CO_2$ to
696 investigate emissions from vehicles: Evidence for an impact of ambient temperature and
697 specific humidity. *Atmospheric Environment*, *232*(x), 117558.
698 https://doi.org/10.1016/j.atmosenv.2020.117558

699 Harkins, C., McDonald, B. C., Henze, D. K., & Wiedinmyer, C. (2021). A fuel-based method for
700 updating mobile source emissions during the COVID-19 pandemic. *Environmental*
701 *Research Letters*, *16*(6). https://doi.org/10.1088/1748-9326/ac0660

702 Hickman, J., Hassel, D., Joumard, R., Samaras, Z., & Sorenson, S. (1999). *Methodology for*
703 *Calculating Transport Emissions and Energy Consumption*.
704 https://trimis.ec.europa.eu/sites/default/files/project/documents/meet.pdf

705 Hudda, N., Simon, M. C., Patton, A. P., & Durant, J. L. (2020). Reductions in traffic-related
706 black carbon and ultrafine particle number concentrations in an urban neighborhood during

the COVID-19 pandemic. *Science of The Total Environment*, *742*. https://doi.org/https://doi.org/10.1016/j.scitotenv.2020.140931

Jiang, Y., Tan, Y., Yang, J., Karavalakis, G., Johnson, K. C., Yoon, S., Herner, J., & Durbin, T. D. (2022). Understanding elevated real-world $NO_x$ emissions: Heavy-duty diesel engine certification testing versus in-use vehicle testing. *Fuel*, *307*. https://doi.org/https://doi.org/10.1016/j.fuel.2021.121771

Joshi, A., James, S., Meckl, P., King, G., Laboratories, R., & Jennings, K. (2009). Assessment of Charge-Air Cooler Health in Diesel Engines Using Nonlinear Time Series Analysis of Intake Manifold Temperature. *Journal of Dynamic Systems Measurement and Control*, *131*(4). https://doi.org/10.1115/1.3023142

Kean, A. J., Harley, R. A., & Kendall, G. R. (2003). Effects of Vehicle Speed and Engine Load on Motor Vehicle Emissions. *Environmental Science & Technology*, *37*(17), 3739–3746. https://doi.org/10.1021/es0263588

Kim, E., & Hopke, P. K. (2012). Source Apportionment of Fine Particles in Washington, DC, Utilizing Temperature-Resolved Carbon Fractions. *Journal of the Air & Waste Management Association*, *54*(7), 773–785. https://doi.org/10.1080/10473289.2004.10470948

Kondo, Y., Komazaki, Y., Miyazaki, Y., Moteki, N., Takegawa, N., Kodama, D., Deguchi, S., Nogami, M., Fukuda, M., Miyakawa, T., Morino, Y., Koike, M., Sakurai, H., & Ehara, K. (2006). Temporal variations of elemental carbon in Tokyo. *Journal of Geophysical Research*, *111*(D12205). https://doi.org/https://doi.org/10.1029/2005JD006257

Krecl, P., Targino, A. C., Landi, T. P., & Ketzel, M. (2018). Determination of black carbon, $PM_{2.5}$ particle number and $NO_x$ emission factors from roadside measurements and their

implications for emission inventory development. *Atmospheric Environment*, *186*, 229–240. https://doi.org/https://doi.org/10.1016/j.atmosenv.2018.05.042

Krüger, O. O., Holanda, B. A., Chowdhury, S., Pozzer, A., Walter, D., Pöhlker, C., Andrés Hernández, M. D., Burrows, J. P., Voigt, C., Lelieveld, J., Quaas, J., Pöschl, U., & Pöhlker, M. L. (2022). Black carbon aerosol reductions during COVID-19 confinement quantified by aircraft measurements over Europe. *Atmos. Chem. Phys.*, *22*(13), 8683–8699. https://doi.org/10.5194/acp-22-8683-2022

Laughner, J. L., Neu, J. L., Schimel, D., Wennberg, P. O., Barsanti, K., Bowman, K. W., Chatterjee, A., Croes, B. E., Fitzmaurice, H. L., Henze, D. K., Kim, J., Kort, E. A., Liu, Z., Miyazaki, K., Turner, A. J., Anenberg, S., Avise, J., Cao, H., Crisp, D., … Zeng, Z.-C. (2021). Societal shifts due to COVID-19 reveal large-scale complexities and feedbacks between atmospheric chemistry and climate change. *Proceedings of the National Academy of Sciences*, *118*(46), e2109481118. https://doi.org/10.1073/pnas.2109481118

Li, P., & Lü, L. (2021). Research on a China 6b heavy-duty diesel vehicle real-world engine out $NO_x$ emission deterioration and ambient correction using big data approach. *Environmental Science and Pollution Research International*. https://doi.org/10.1007/s11356-021-15778-2

Lopez-Coto, I., Ren, X., Karion, A., McKain, K., Sweeney, C., Dickerson, R. R., McDonald, B. C., Ahn, D. Y., Salawitch, R. J., He, H., Shepson, P. B., & Whetstone, J. R. (2022). Carbon Monoxide Emissions from the Washington, DC, and Baltimore Metropolitan Area: Recent Trend and COVID-19 Anomaly. *Environmental Science & Technology*, *56*(4), 2172–2180. https://doi.org/10.1021/acs.est.1c06288

Lyu, Y., & Olofsson, U. (2020). On black carbon emission from automotive disc brakes. *Journal*

751 *of Aerosol Science*, *148*, 105610.
752 https://doi.org/https://doi.org/10.1016/j.jaerosci.2020.105610

753 McCaffery, C., Zhu, H., Tang, T., Li, C., Karavalakis, G., Cao, S., Oshinuga, A., Burnette, A.,
754 Johnson, K. C., & Durbin, T. D. (2021). Real-world $NO_x$ emissions from heavy-duty diesel,
755 natural gas, and diesel hybrid electric vehicles of different vocations on California
756 roadways. *Science of The Total Environment*, *784*.
757 https://doi.org/https://doi.org/10.1016/j.scitotenv.2021.147224

758 Naser, T. M., Kanda, I., Ohara, T., Sakamoto, K., Kobayashi, S., Nitta, H., & Nataami, T.
759 (2009). Analysis of traffic-related $NO_x$ and EC concentrations at various distances from
760 major roads in Japan. *Atmospheric Environment*, *43*(15), 2379–2390.
761 https://doi.org/https://doi.org/10.1016/j.atmosenv.2009.02.002

762 O'Driscoll, R., Stettler, M., Molden, N., Oxley, T., & Apsimon, H. (2018). Real world $CO_2$ and
763 $NO_x$ emissions from 149 Euro 5 and 6 diesel, gasoline and hybrid passenger cars. *The*
764 *Science of the Total Environment*, *621*, 282–290.
765 https://doi.org/10.1016/j.scitotenv.2017.11.271

766 OECD, & ECMT. (2006). *Speed Management*. https://www.itf-
767 oecd.org/sites/default/files/docs/06speed.pdf

768 Park, S. S., Kozawa, K., Fruin, S., Mara, S., Hsu, Y.-K., Jakober, C., Winer, A., & Herner, J.
769 (2011). Emission Factors for High-Emitting Vehicles Based on On-Road Measurements of
770 Individual Vehicle Exhaust with a Mobile Measurement Platform. *Journal of the Air &*
771 *Waste Management Association*, *61*(10), 1046–1056.
772 https://doi.org/10.1080/10473289.2011.595981

773 Pusede, S. E., & Cohen, R. C. (2012). On the observed response of ozone to $NO_x$ and VOC
774 reactivity reductions in San Joaquin Valley California 1995-present. *Atmospheric Chemistry*
775 *and Physics*, *12*(18), 8323–8339. https://doi.org/10.5194/acp-12-8323-2012

776 Rakopoulos, C., & Giakoumis, E. (2009). *Diesel Engine Transient Operation*.
777 https://doi.org/10.1007/978-1-84882-375-4

778 Saha, P. K., Khlystov, A., Snyder, M. G., & Grieshop, A. P. (2018). Characterization of air
779 pollutant concentrations, fleet emission factors, and dispersion near a North Carolina
780 interstate freeway across two seasons. *Atmospheric Environment*, *177*(January), 143–153.
781 https://doi.org/10.1016/j.atmosenv.2018.01.019

782 Sather, M. E., & Cavender, K. (2016). Trends analyses of 30 years of ambient 8 hour ozone and
783 precursor monitoring data in the South Central U.S.: progress and challenges. *Environ. Sci.:*
784 *Processes & Impacts*, *18*(7), 819–831. https://doi.org/10.1039/C6EM00210B

785 Schauer, J. J., Christensen, C. G., Kittelson, D. B., Johnson, J. P., & Watts, W. F. (2008). Impact
786 of Ambient Temperatures and Driving Conditions on the Chemical Composition of
787 Particulate Matter Emissions from Non-Smoking Gasoline-Powered Motor Vehicles.
788 *Aerosol Science and Technology*, *42*(3), 210–223.
789 https://doi.org/10.1080/02786820801958742

790 Sher, E. (Ed.). (1998). Chapter 10: Combustion-Related Emissions in CI Engines. In *Handbook*
791 *of Air Pollution from Internal Combustion Engines: Pollutant Formation and Control* (1st
792 Editio). Academic Press.

793 US Department of Transportation Federal Highway Administration. (2014). *Verification,*
794 *Refinement, and Applicability of Long-Term Pavement Performance Vehicle Classification*

*Rules*.
https://www.fhwa.dot.gov/publications/research/infrastructure/pavements/ltpp/13091/002.cfm

US EPA. (2015a). *Emission Adjustments for Temperature , Humidity , Air Conditioning , and Inspection and Maintenance for On - road Vehicles in MOVES2014*. https://www.epa.gov/moves/moves-technical-reports

US EPA. (2015b). *MOVES2014a User Guide*. https://www.epa.gov/moves/moves2014a-latest-version-motor-vehicle-emission-simulator-moves

US EPA. (2016). *Integrated Review Plan for the National Ambient Air Quality Standards for Particulate Matter*. https://www3.epa.gov/ttn/naaqs/standards/pm/data/201612-final-integrated-review-plan.pdf

US EPA. (2020a). *Emission Adjustments for Temperature, Humidity, Air Conditioning and Inspection and Maintenance for Onroad Vehicles in MOVES3*. https://nepis.epa.gov/Exe/ZyPDF.cgi?Dockey=P1010M29.pdf

US EPA. (2020b). *The 2019 EPA Automotive Trends Report*. https://nepis.epa.gov/Exe/ZyPDF.cgi?Dockey=P100YVFS.pdf

US EPA. (2021a). *Basics of Climate Change*. https://www.epa.gov/climatechange-science/basics-climate-change#aerosols

US EPA. (2021b). *Particulate Matter (PM) Basics*. https://www.epa.gov/pm-pollution/particulate-matter-pm-basics#effects

US EPA. (2021c). *Regional Fuels and the Fuel Wizard in MOVES3* (pp. 1–67).

https://nepis.epa.gov/Exe/ZyPDF.cgi?Dockey=P10119R7.pdf

US EPA. (2022). *2017 National Emissions Inventory (NEI) Data*. https://www.epa.gov/air-emissions-inventories/2017-national-emissions-inventory-nei-data

Vaisala. (2012). *Vaisala Weather Transmitter WXT 520*. https://www.vaisala.com/sites/default/files/documents/M210906EN-C.pdf

Wang, J. M., Jeong, C. H., Hilker, N., Shairsingh, K. K., Healy, R. M., Sofowote, U., Debosz, J., Su, Y., McGaughey, M., Doerksen, G., Munoz, T., White, L., Herod, D., & Evans, G. J. (2018). Near-Road Air Pollutant Measurements: Accounting for Inter-Site Variability Using Emission Factors. *Environmental Science and Technology*, *52*(16), 9495–9504. https://doi.org/10.1021/acs.est.8b01914

Weber, C., Sundvor, I., & Figenbaum, E. (2019). Comparison of regulated emission factors of Euro 6 LDV in Nordic temperatures and cold start conditions : Diesel- and gasoline direct-injection. *Atmospheric Environment*, *206*, 208–217. https://doi.org/10.1016/j.atmosenv.2019.02.031

Yadav, V., Ghosh, S., Mueller, K., Karion, A., Roest, G., Gourdji, S. M., Lopez-Coto, I., Gurney, K. R., Parazoo, N., Verhulst, K. R., Kim, J., Prinzivalli, S., Fain, C., Nehrkorn, T., Mountain, M., Keeling, R. F., Weiss, R. F., Duren, R., Miller, C. E., & Whetstone, J. (2021). The Impact of COVID-19 on $CO_2$ Emissions in the Los Angeles and Washington DC/Baltimore Metropolitan Areas. *Geophysical Research Letters*, *48*(11). https://doi.org/https://doi.org/10.1029/2021GL092744

Yang, J., Wen, Y., Wang, Y., Zhang, S., Pinto, J. P., Pennington, E. A., Wang, Z., Wu, Y., Sander, S. P., Jiang, J. H., Hao, J., Yung, Y. L., & Seinfeld, J. H. (2021). From COVID-19

to future electrification: Assessing traffic impacts on air quality by a machine-learning model. *Proceedings of the National Academy of Sciences*, *118*(26). https://doi.org/10.1073/pnas.2102705118

Zeng, N., Han, P., Liu, Z., Liu, D., Oda, T., Martin, C., Liu, Z., Yao, B., Sun, W., Wang, P., Cai, Q., Dickerson, R., & Maksyutov, S. (2022). Global to local impacts on atmospheric $CO_2$ from the COVID-19 lockdown, biosphere and weather variabilities. *Environmental Research Letters*, *17*(1), 15003. https://doi.org/10.1088/1748-9326/ac3f62